Hindawi
Mathematical Problems in Engineering
Volume 2020, Article ID 3657848, 7 pages
https://doi.org/10.1155/2020/3657848

Research Article

Fractional-Order Active Disturbance Rejection Controller for Motion Control of a Novel 6-DOF Parallel Robot

Xinxin Shi,[1] **Jiacai Huang**,[2] **and Fangzheng Gao**[1]

[1]*School of Automation, Nanjing Institute of Technology, No. 1 Hongjing Road, Nanjing 211167, China*
[2]*Industrial Center, Nanjing Institute of Technology, No. 1 Hongjing Road, Nanjing 211167, China*

Correspondence should be addressed to Xinxin Shi; sxx@njit.edu.cn

Received 9 August 2020; Revised 11 September 2020; Accepted 17 December 2020; Published 29 December 2020

Academic Editor: Libor Pekař

A novel 6-degree-of-freedom (6-DOF) parallel robot driven by six novel linear motors is designed and controlled in this paper. Detailed structures of linear motors are illustrated. A control strategy based on kinematics of the 6-DOF parallel robot is used, and six linear motors are controlled to track their own desired trajectories under a designed fractional-order active disturbance rejection controller (FOADRC). Compared with the normal ADRC, two desired trajectories and three different working situations of a linear motor are simulated to show good performances of the FOADRC. Experimental results show that six linear motors can track their own desired trajectories accurately under payloads and disturbances, and the novel 6-DOF parallel robot can be controlled well.

1. Introduction

Industrial robots have two main types, i.e., serial and parallel robots. Each type of robot has its own advantages and disadvantages. Advantages of serial robots are simple structures, convenient control, and large workspace. Compared with serial counterparts, parallel robots have advantages of large loading capacity, high-speed and high-precision motions, and strong stiffness [1, 2]. With these superior characteristics, parallel robots have many industrial applications nowadays, such as pick-and-place [3], docking simulator [4], and medical surgery [5].

Besides their own mechanical structures, the joint-driven ways are the very important aspects of parallel robots. There are different kinds of actuators to drive joints in parallel robots, such as cables [6], pneumatic or hydraulic cylinders [7], and rotary motors [8]. In this paper, a novel 6-DOF robot, which is actually a manipulator, was designed and driven by self-made linear motors. There is no need to use additional mechanisms such as ball screws to realize linear motions, and therefore, the whole system structure can be simplified.

Control technologies of parallel robots are also very important, especially for the direct-drive actuators since uncertain system disturbances will act on them directly [9, 10]. Control methods of parallel robots can be classified based on kinematics and dynamics [11, 12]. Dynamics-based control methods require accurate dynamical models of parallel robots. In practice, there is inevitably an error between the established dynamical model and the real system. This error will lead to a decrease in the control performance [13, 14]. In addition, parameter values of dynamical models of parallel robots are not fixed, and they are constantly updated with movements of robots, which brings heavy calculations and higher requirements on the computing power of the controller hardware.

Kinematics-based control methods assume that actuators of parallel robots are independent of each other [15]. By controlling each actuator to track their target trajectory, the desired trajectory and posture of the robot are achieved [16]. The kinematics-based control method is essentially the same as the design method of the single-axis motion controller. There is no need to consider the dynamical model of a parallel robot. It is simple to implement. However, in practical applications, actuators are not independent of each other. They are coupled with each other through the manipulator, and the moving manipulator acts on each actuator with constantly changing load forces. Therefore,

performances of the kinematics-based control method depends heavily on the antidisturbance capability of the single-axis motion controller.

To achieve high-performance motion control, a model predictive control was studied on a 5-DOF parallel robot in [17], and a modified robust control was designed in [18] for a 2-DOF parallel robot. Fractional robust control methods were proposed for a delta parallel robot in [19]. Disturbance observer (DOB) is a useful tool for motion control [20, 21]. An adaptive sliding-mode control based on a DOB was applied well on a manipulator in [22]. Parameter uncertainties can be seen as system disturbances, and a novel control strategy was designed to compensate nonlinear dynamics and model uncertainties of a long-stroke hydraulic robot [23].

This paper adopts a control strategy based on kinematics and proposes the FOADRC, which effectively improves the disturbance rejection capability and trajectory tracking accuracy of each linear so that the novel 6-DOF parallel robot can achieve the given target motion better. Compared with other controllers such as fractional-order sliding-mode control [24], fuzzy and recurrent neural network [25], and dynamic terminal sliding-mode control [26], main differences of the proposed method are that accurate system models are not needed to obtain in advance, and it can be applied to practice easily. Modelling errors, parameter uncertainties, and external disturbances are estimated as the total disturbance which can be compensated online. However, control accuracy of the proposed method needs improvement.

The proposed FOADRC is based on the conventional ADRC. In [27], details of the conventional ADRC are analyzed, including the stability. ADRC is a practical control strategy which has been used in many applications, such as coal-fired power plant [28], precise position tracking control [29], and gasoline engines [30]. In this proposed FOADRC, the component nonlinear PD is substituted by FOPD. FOPD is first validated stable and useful by experiments in [31]. Therefore, it can be concluded that the FOADRC is also stable. In addition, simulation and experimental results show that the proposed FOADRC is effective in practice.

1.1. Details of the Parallel Robot. The novel 6-DOF parallel robot is given in Figure 1, which has components of six novel linear motors numbered 1 to 6, a motion plate and a base plate connected by rods and hinges, and an attitude sensor.

Linear motors are the main actuators of this 6-DOF parallel robot. Details of the linear motor are demonstrated in Figure 2. The linear motor is modelled as the following equation:

$$\begin{cases} L\dot{i} = -Ri - K_e\dot{x} + u(\Sigma i), \\ m\ddot{x} = -F + K_f i(\Sigma x), \\ F = F_f + F_r + F_d, \end{cases} \tag{1}$$

where u, i, L, and R are the phase voltage, current, inductance, and resistance, x and m are the displacement and mass of the moving part, K_e and K_f are the back electromotive force coefficient and electromagnetic force coefficient, respectively, F_f is the friction, and F_d is the disturbances, including the interaction forces between linear motors and external disturbances.

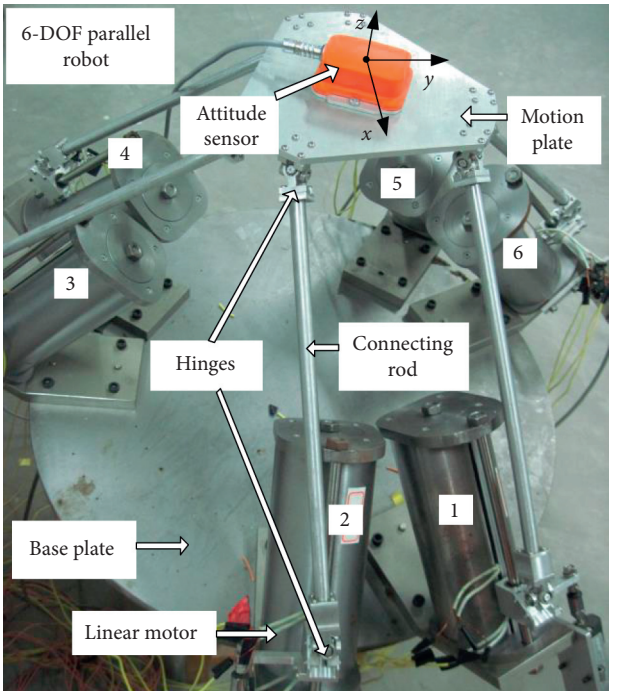

Figure 1: Prototype of novel 6-DOF parallel robot.

2. FOADRC and Motion Control System

2.1. Motion Control System of Linear Motor. Here, a kinematics-based control strategy is adopted for the novel 6-DOF parallel robot, that is, six linear motors are controlled to track their own trajectories independently, and interactions among different linear motors are dealt with as disturbances. Therefore, a control system of one linear motor is constructed firstly based on the FOADRC, as illustrated in Figure 3.

2.2. Details of FOADRC. There are three important components in the FOADRC, i.e., a tracking differentiator (TD), a fractional-order PD (FOPD), and an extended state observer (ESO). TD is expressed as the following equations in [27]:

$$\begin{cases} \dot{x}_1 = x_2, \\ \dot{x}_2 = \text{fhan}(x_1 - x_d, x_2, r, h_0), \end{cases} \tag{2}$$

where x_d is the given position, x_1 is the transition process of x_d, and x_2 is the velocity.

$$\text{fhan}(x_1 - x_d, x_2, r, h_0) = \begin{cases} -r \cdot \text{sgn}(a), & |a| > d \\ -r \cdot \dfrac{a}{d}, & |a| \le d \end{cases} \tag{3}$$

ESO is expressed as in the following equation:

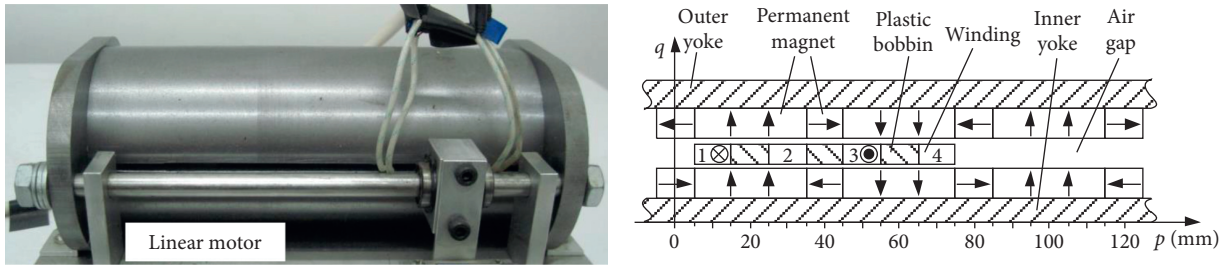

(a) (b)

Figure 2: Details of the linear motor. (a) Appearance. (b) Internal structure.

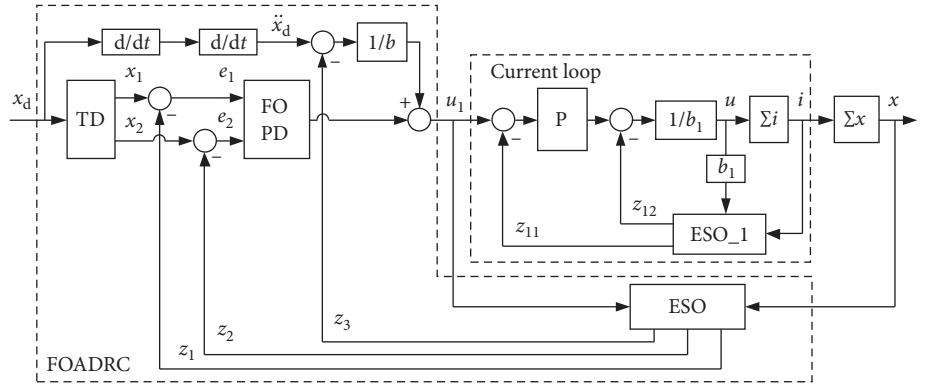

Figure 3: Motion control of the linear motor based on FOADRC.

$$\begin{cases} e = z_1 - x, \\ \dot{z}_1 = z_2 - \beta_{01} \cdot e, \\ \dot{z}_2 = z_3 - \beta_{02} \cdot \mathrm{fal}(e, 0.5, \delta) + b \cdot u, \\ \dot{z}_3 = -\beta_{03} \cdot \mathrm{fal}(e, 0.25, \delta), \end{cases} \tag{4}$$

where β_{01}, β_{02}, and β_{03} are ESO gains which can be selected as the following equation in [27]:

$$\beta_{01} \approx \frac{1}{h}, \beta_{02} \approx \frac{1}{1.6h^{1.5}}, \beta_{03} \approx \frac{1}{8.6h^{2.2}}. \tag{5}$$

$\mathrm{fal}(e, \alpha, \delta)$ is given as the following equation:

$$\mathrm{fal}(e, \alpha, \delta) = \begin{cases} e \cdot \delta^{\alpha - 1}, & |e| \le \delta, \\ |e|^{\alpha} \cdot \mathrm{sgn}(e), & |e| > \delta. \end{cases} \tag{6}$$

FOPD is expressed as the following equation:

$$G(s) = K_p(1 + K_d s^{\mu}), \tag{7}$$

where μ is a fraction between 0 and 1 and K_p and K_d are the controller gains.

ESO_1 is given in the following equation:

$$\begin{cases} e = z_{11} - i, \\ \dot{z}_{11} = z_{12} - \beta_{11} \cdot e + b_1 \cdot u, \\ \dot{z}_{12} = -\beta_{12} \cdot \mathrm{fal}(e, 0.5, \delta_1), \end{cases} \tag{8}$$

where β_{11}、β_{12}, and b_1 are the parameters of the ESO_1.

3. Comparative Simulations

3.1. Comparative Controller Details. Compared with the normal active disturbance rejection controller (ADRC), two designed trajectories and three different working situations of a linear motor are simulated to demonstrate good performances of the FOADRC in the MATLAB/Simulink software. Detailed parameters of the linear motor and the FOADRC are given in Tables 1 and 2. K_{p1} is the P controller gain in the current loop, and h and h_1 are the sampling intervals of ESO and ESO_1, respectively.

Two desired trajectories are given in the following equation:

$$x_d = \begin{cases} 5\sin(5t - 0.5\pi) + 5\,(\mathrm{mm}), S1, \\ 20\sin(7t - 0.5\pi) + 20\,(\mathrm{mm}), S2. \end{cases} \tag{9}$$

3.2. Simulation Results under Different Situations. Three different working situations are compared: without payloads, with parameter variations, and with external disturbances. Comparative results without payloads are illustrated in Figure 4.

To test the system robustness, a 7.75 kg mass is loaded and results are compared in Figure 5. A disturbance force of 8 N acts on the system between 0.6 s and 1.2 s, and comparative results are illustrated in Figure 6.

Figures 4–6 show that the FOADRC performs well under payloads and disturbances, and the control accuracy is higher than ADRC.

Table 1: Parameters of the linear motor.

Parameters	R (Ω)	L (mH)	M (g)	K_f/(N/A)	K_e/(Vs/m)
Values	3.4	4.42	250	18.01	18.01

Table 2: Parameters of FOADRC.

Parameters	Values	Parameters	Values
h_0	0.000 2	β_{01}	5000
h	0.000 2	β_{02}	220970
h_1	0.000 025	β_{03}	15967450
b_1	226	δ	0.000 2
β_{11}	40000	μ	0.835
β_{12}	5000000	K_{p1}	40 000
δ_1	0.000025	B	72
K_p	100 000	K_d	300

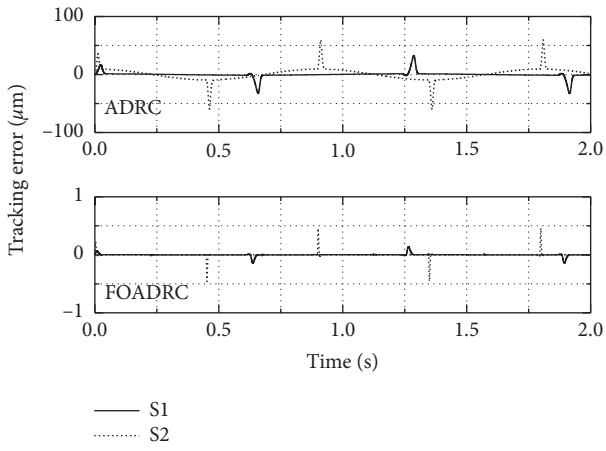

Figure 4: Comparative results without payloads.

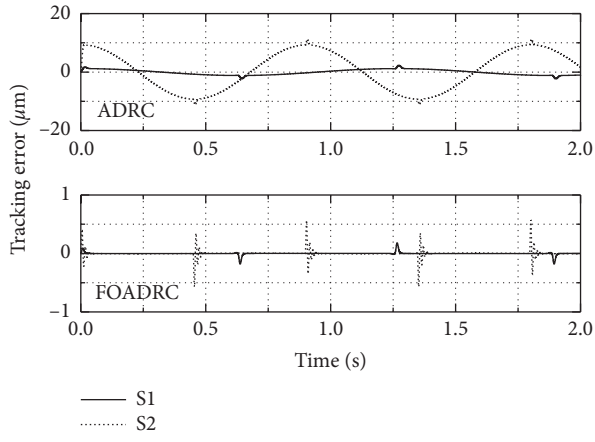

Figure 5: Comparative results with payloads.

4. Experimental Validations and Discussion

4.1. Experimental Prototype. An experimental setup of the novel 6-DOF parallel robot on the basis of a dSPACE real-time hardware-in-loop system was constructed as given in Figure 7. The experimental setup is composed of dSPACE modular hardware boards (DS1005, DS4002, and DS2004), driving modules, current sensors, displacement sensors, attitude sensor, 6-DOF parallel robot, and personal computer (PC). The software running in the PC is used to realize the real-time simulation model of the control system, display the operating parameters of the system, and adjust the parameters of the controller in real time. DS1005 is the core of the real-time control system. DS4002 and DS2004 are connected to DS1005 through the external device high-speed bus peripheral high speed (PHS) for data communication.

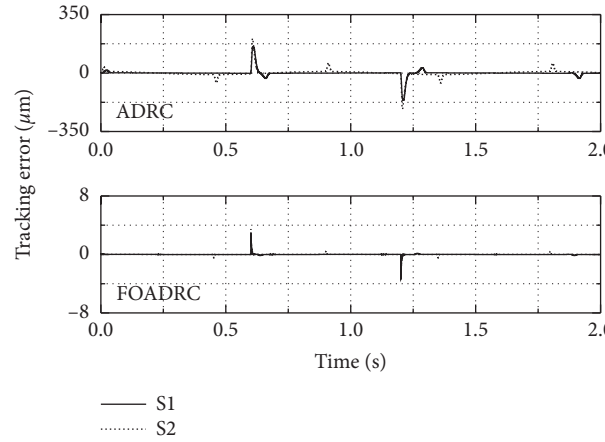

Figure 6: Comparative results with disturbances.

The double-loop series closed-loop hall current sensor TBC05SY and KTM series sliding variable resistance linear displacement sensor are selected. Both of the sensor linearity is 0.1%. Each linear motor is driven by its own driving module. The attitude sensor is used to measure the pose of the motion plate, including the rotation angle around the x-, y-, and z-axes. The measured data are sent to the MT Manager software for real-time display. Current sensors collect winding current signals of linear motors and send them to the analog-to-digital conversion board DS2004, and conversion results are sent to the main control board DS1005 to calculate control inputs. Pulse-width-modulation (PWM) signals are generated by the DS4002 board and the PWM frequency is 40 kHz.

5. Results and Discussion

Suppose the desired motion of the robot is in the following equation:

$$\begin{cases} \theta_x = 1.915\sin(3.749t) + 6.577\cos(3.749t) + 5.558\,(^\circ), \\ \theta_y = -5.024\sin(3.749t) - 0.965\cos(3.749t) + 0.313\,(^\circ), \\ \theta_z = 3.449\sin(3.749t) - 0.418\cos(3.749t) - 3.202\,(^\circ), \end{cases} \tag{10}$$

where θ_x, θ_y, and θ_z are the angles around three different axes, as shown in Figure 1. Desired trajectories of six linear motors are calculated as in the following equation:

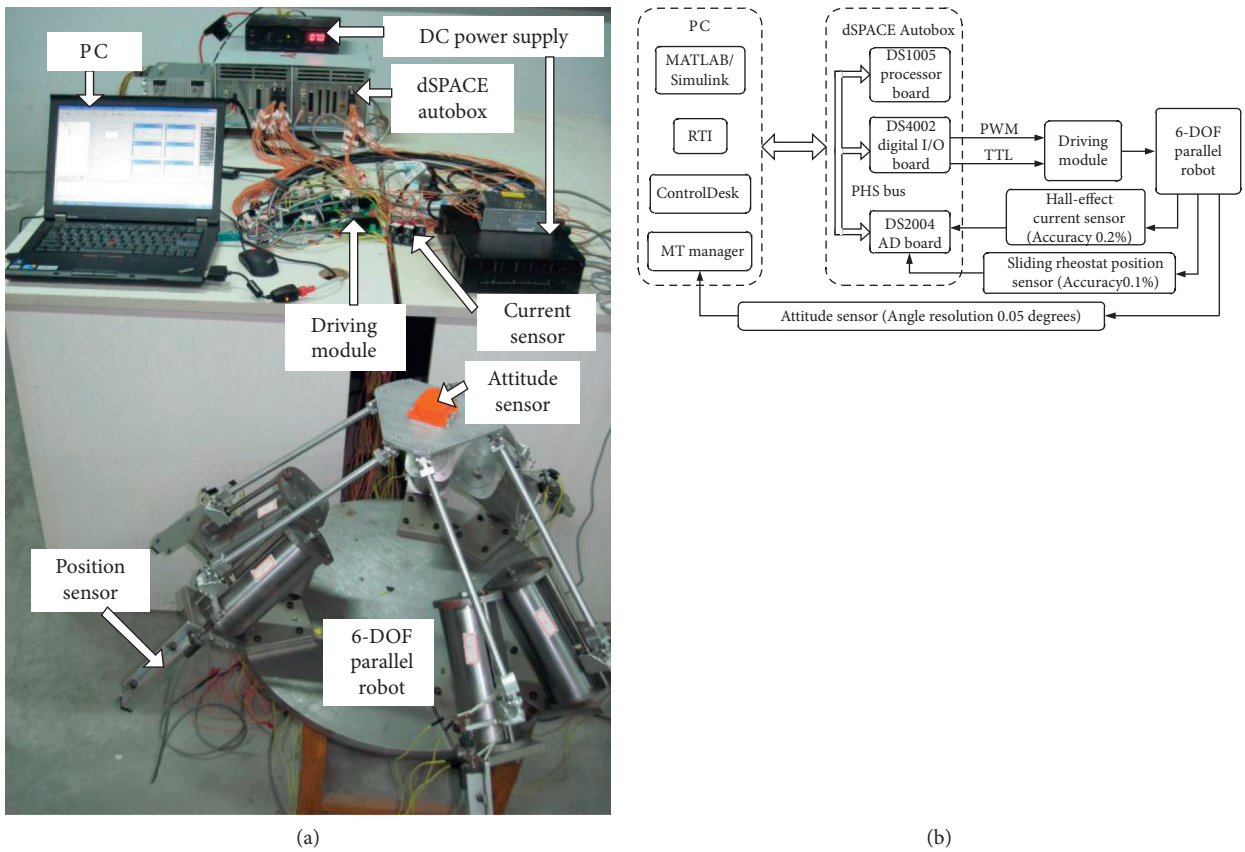

Figure 7: Experimental setup of 6-DOF parallel robot. (a) Actual. (b) Logical.

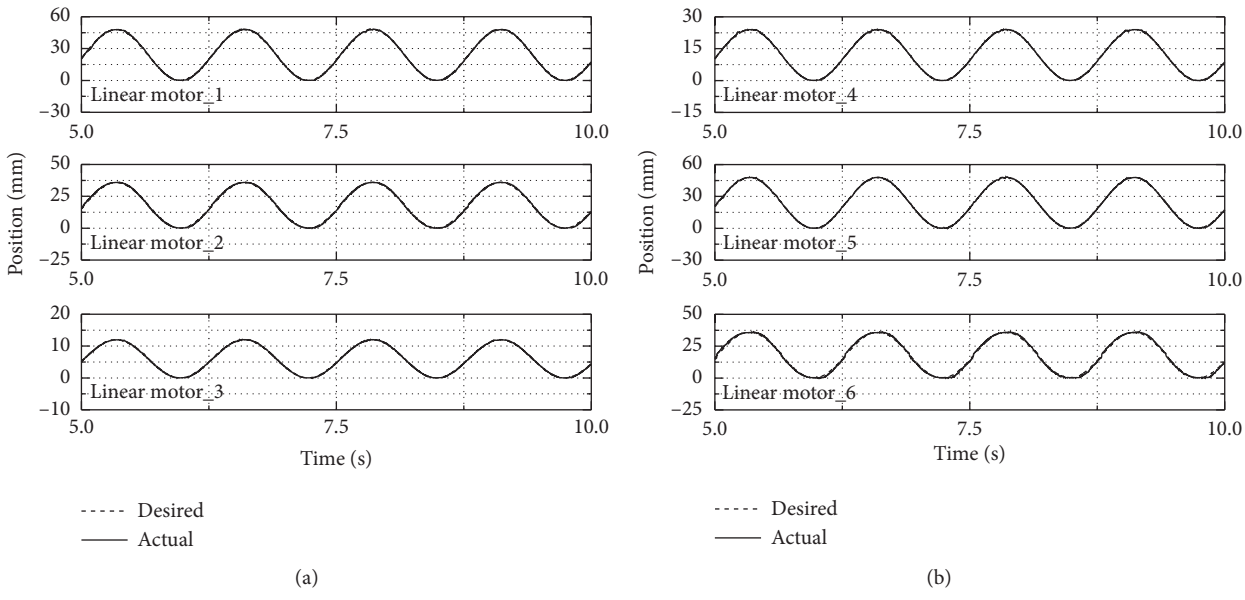

Figure 8: Actual tracking results. (a) Linear motor nos. 1–3. (b) Linear motor nos. 4–6.

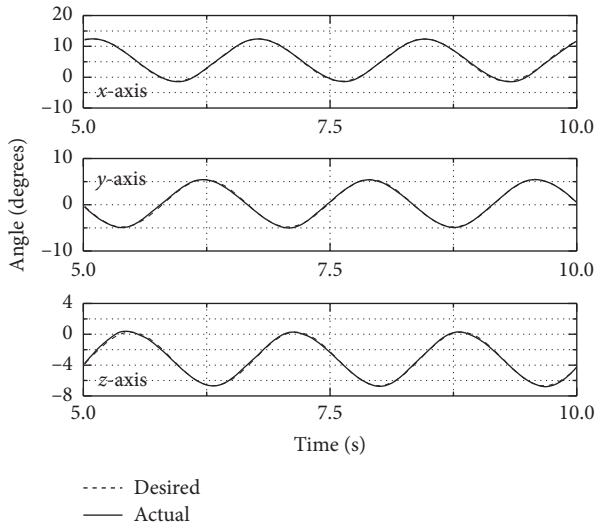

Figure 9: Motion performance of the robot.

$$\begin{cases} x_{d1} = 24\sin(5t) + 24\,(\text{mm}), \\ x_{d2} = 18\sin(5t) + 18\,(\text{mm}), \\ x_{d3} = 6\sin(5t) + 6\,(\text{mm}), \\ x_{d4} = 12\sin(5t) + 12\,(\text{mm}), \\ x_{d5} = 24\sin(5t) + 24\,(\text{mm}), \\ x_{d6} = 18\sin(5t) + 18\,(\text{mm}). \end{cases} \tag{11}$$

Actual tracking results are given in Figures 8 and 9. It can be seen from Figures 8 and 9 that six linear motors track their desired trajectories well, and the novel 6-DOF parallel robot is driven to reach its control goal. Effectiveness of the FOADRC is verified by experiments.

ESO is an important part of the FOADRC, which can be realized in the actual test. However, due to the limitation of the measurement accuracy of sensors, the observation effect of the ESO is not very good. The trajectory tracking accuracy in the experiment is not as good as that of the simulation. High-resolution current and displacement sensors can be chosen, such as optical encoders, to further improve the control performance.

6. Conclusions

A FOADRC is proposed in this paper, and it is implemented on a novel 6-DOF parallel robot for actual test. A kinematics-based control method is adopted to realize desired motions of this 6-DOF parallel robot. Six linear motors are controlled to track their own trajectories independently, and interactions among different linear motors are dealt with as disturbances. Different trajectories and working situations of a linear motor are simulated to demonstrate good performances of the FOADRC. Compared with the normal ADRC, the designed FOADRC can improve the system trajectory tracking performance effectively. Due to limitations of working space and singularity problem of the parallel robot, only sinusoidal trajectory tracking control is analyzed at present. In future work, we will further optimize the motion platform and conduct control research on various motion trajectories to promote the application of this 6-DOF parallel robot in industrial practice.

Data Availability

The data used to support the findings of this study are available from the corresponding author upon request.

Conflicts of Interest

The authors declare that there are no conflicts of interest.

Acknowledgments

This work was supported by the Scientific Research Foundation of Nanjing Institute of Technology (grant no. CKJA201903); the National Natural Science Foundation of China (grant nos. 51505213 and 61873120); and the QingLan Project of Jiangsu Province.

References

[1] H. S. Kim, Y. M. Cho, and K.-I. Lee, "Robust nonlinear task space control for 6 DOF parallel manipulator," *Automatica*, vol. 41, no. 9, pp. 1591–1600, 2005.

[2] H. Abdellatif and B. Heimann, "Advanced model-based control of a 6-DOF hexapod robot: a case study," *IEEE/ASME Transactions on Mechatronics*, vol. 15, no. 2, pp. 269–279, 2010.

[3] B. Belzile, P. K. Eskandary, and J. Angeles, "Workspace determination and feedback control of a pick-and-place parallel robot: analysis and experiments," *IEEE Robotics and Automation Letters*, vol. 5, no. 1, pp. 40–47, 2020.

[4] Q. Wang, C. Qi, F. Gao, X. Zhao, A. Ren, and Y. Hu, "Normal contact stiffness identification-based force compensation for a hardware-in-the-loop docking simulator," *Advanced Robotics*, vol. 32, no. 5, pp. 266–282, 2018.

[5] C. Li, X. Gu, X. Xiao, C. M. Lim, and H. Ren, "A Robotic system with multichannel flexible parallel manipulators for single port access surgery," *IEEE Transactions on Industrial Informatics*, vol. 15, no. 3, pp. 1678–1687, 2019.

[6] H. Choi, J. Piao, E.-S. Kim et al., "Intuitive bilateral teleoperation of a cable-driven parallel robot controlled by a cable-driven parallel robot," *International Journal of Control, Automation and Systems*, vol. 18, no. 7, pp. 1792–1805, 2020.

[7] M. Taghizadeh and M. Javad Yarmohammadi, "Development of a self-tuning PID controller on hydraulically actuated stewart platform stabilizer with base excitation," *International Journal of Control, Automation and Systems*, vol. 16, no. 6, pp. 2990–2999, 2018.

[8] K. Kuhnlenz and B. Kuhnlenz, "Motor interference of incongruent motions increases workload in close HRI," *Advanced Robotics*, vol. 34, no. 6, pp. 400–406, 2020.

[9] B. Lu, Y. Fang, and N. Sun, "Continuous sliding mode control strategy for a class of nonlinear underactuated systems," *IEEE Transactions on Automatic Control*, vol. 63, no. 10, pp. 3471–3478, 2018.

[10] X. Liang, Y. Wan, and C. Zhang, "Task space trajectory tracking control of robot manipulators with uncertain kinematics and dynamics," *Mathematical Problems in Engineering*, vol. 2017, Article ID 4275201, 19 pages, 2017.

[11] T. Sun, D. Liang, and Y. Song, "Singular-perturbation-based nonlinear hybrid control of redundant parallel robot," *IEEE Transactions on Industrial Electronics*, vol. 65, no. 4, pp. 3326–3336, 2018.

[12] R.-J. Lian, "Intelligent controller for robotic motion control," *IEEE Transactions on Industrial Electronics*, vol. 58, no. 11, pp. 5220–5230, 2011.

[13] O. Koc, G. Maeda, and J. Peters, "Optimizing the execution of dynamic robot movements with learning control," *IEEE Transactions on Robotics*, vol. 35, no. 4, pp. 909–924, 2019.

[14] P. Wang, D. Zhang, and B. Lu, "Robust fuzzy sliding mode control based on low pass filter for the welding robot with dynamic uncertainty," *Industrial Robot*, vol. 47, no. 1, pp. 111–120, 2020.

[15] Y. Jin, I.-M. Chen, and G. Yang, "Kinematic design of a 6-DOF parallel manipulator with decoupled translation and rotation," *IEEE Transactions on Robotics*, vol. 22, no. 3, pp. 545–551, 2006.

[16] Y. Wang, Q. Lin, L. Zhou, X. Shi, and L. Wang, "Backstepping sliding mode robust control for a wire-driven parallel robot based on a nonlinear disturbance observer," *Mathematical Problems In Engineering*, vol. 2020, Article ID 3146762, p. 17, 2020.

[17] S. Wen, G. Qin, B. Zhang, H. K. Lam, Y. Zhao, and H. Wang, "The study of model predictive control algorithm based on the force/position control scheme of the 5-DOF redundant actuation parallel robot," *Robotics and Autonomous Systems*, vol. 79, pp. 12–25, 2016.

[18] X. Yang, L. Zhu, Y. Ni et al., "Modified robust dynamic control for a diamond parallel robot," *IEEE/ASME Transactions on Mechatronics*, vol. 24, no. 3, pp. 959–968, 2019.

[19] R. Zhao, L. Wu, and Y.-H. Chen, "Robust control for nonlinear delta parallel robot with uncertainty: an online estimation approach," *IEEE Access*, vol. 8, pp. 97604–97617, 2020.

[20] W.-H. Chen, J. Yang, L. Guo, and S. Li, "Disturbance-observer-based control and related methods-an overview," *IEEE Transactions on Industrial Electronics*, vol. 63, no. 2, pp. 1083–1095, 2016.

[21] A. Mohammadi, M. Tavakoli, H. J. Marquez, and F. Hashemzadeh, "Nonlinear disturbance observer design for robotic manipulators," *Control Engineering Practice*, vol. 21, no. 3, pp. 253–267, 2013.

[22] K.-Y. Chen, "Robust optimal adaptive sliding mode control with the disturbance observer for a manipulator robot system," *International Journal of Control, Automation and Systems*, vol. 16, no. 4, pp. 1701–1715, 2018.

[23] Y. Huang, D. M. Pool, O. Stroosma, and Q. Chu, "Long-stroke hydraulic robot motion control with incremental nonlinear dynamic inversion," *IEEE/ASME Transactions on Mechatronics*, vol. 24, no. 1, pp. 304–314, 2019.

[24] J. Fei and Z. Feng, "Fractional-order finite-time super-twisting sliding mode control of micro gyroscope based on double-loop fuzzy neural network," *IEEE Transactions on Systems, Man, and Cybernetics: Systems*, vol. 50, pp. 1–15, 2020.

[25] J. Fei and Y. Chen, "Fuzzy double hidden layer recurrent neural terminal sliding mode control of single-phase active power filter," *IEEE Transactions on Fuzzy Systems*, vol. 28, pp. 1–14, 2020.

[26] J. Fei and Y. Chen, "Dynamic terminal sliding-mode control for single-phase active power filter using new feedback recurrent neural network," *IEEE Transactions on Power Electronics*, vol. 35, no. 9, pp. 9906–9924, 2020.

[27] J. Han, "From PID to active disturbance rejection control," *IEEE Transactions on Industrial Electronics*, vol. 56, no. 3, pp. 900–906, 2009.

[28] L. Sun, Q. Hua, D. Li, L. Pan, Y. Xue, and K. Y. Lee, "Direct energy balance based active disturbance rejection control for coal-fired power plant," *ISA Transactions*, vol. 70, pp. 486–493, 2017.

[29] H.-L. Xing, J.-H. Jeon, K. C. Park, and I.-K. Oh, "Active disturbance rejection control for precise position tracking of ionic polymer-metal composite actuators," *IEEE/ASME Transactions on Mechatronics*, vol. 18, no. 1, pp. 86–95, 2013.

[30] W. Xue, W. Bai, S. Yang, K. Song, Y. Huang, and H. Xie, "ADRC with adaptive extended state observer and its application to air-fuel ratio control in gasoline engines," *IEEE Transactions on Industrial Electronics*, vol. 62, no. 9, pp. 5847–5857, 2015.

[31] H. Li, Y. Luo, and Y. Chen, "A fractional order proportional and derivative (FOPD) motion controller: tuning rule and experiments," *IEEE Transactions on Control Systems Technology*, vol. 18, no. 2, pp. 516–520, 2010.